PNL-SA-17601

PNL-SA--17601

CONF-900403--9

DE90 008623

Received by OSTI

MAR 2 6 1990

GRAIN BOUNDARY CHEMISTRY EFFECTS ON IRRADIATION-ASSISTED STRESS CORROSION CRACKING

S. M. Bruemmer
L. A. Charlot
E. P. Simonen

March 1990

Presented at the
Corrosion 90
Las Vegas, Nevada
~~March~~ April 23-27, 1990

Work supported by
the U. S. Department of Energy
under Contract DE-AC06-76RLO 1830

Pacific Northwest Laboratory
Richland, Washington 99352

DISCLAIMER

GRAIN BOUNDARY CHEMISTRY EFFECTS ON IRRADIATION-ASSISTED STRESS CORROSION CRACKING

S. M. Bruemmer, L. A. Charlot and E. P. Simonen
Pacific Northwest Laboratory
Richland, WA 99352

Abstract

Radiation-induced segregation (RIS) to grain boundaries and interfacial microchemistry effects on intergranular stress corrosion cracking (IGSCC) has been investigated in 304 and 316 stainless steels (SS). Irradiation dose effects on RIS to grain boundaries were studied using nickel ion bombardment of fine-grained, sputter-deposited SS. Damage levels from 1 to 20 dpa were produced in near-surface regions encompassing several grain diameters in depth. The resultant "bulk" damage promoted RIS of silicon and nickel, as well as depletion of chromium at grain interfaces. Maximum enrichment/depletion ratios of about 4.0, 1.1 and 0.7 were measured for silicon, nickel and chromium, respectively. Composition changes were localized to within 20 nm of the boundary as measured by analytical transmission electron microscopy. No grain boundary enrichment of phosphorus was observed in these heats even though heats contained high levels of phosphorus in the bulk.

Grain boundary chemistry effects on the intergranular (IG) corrosion and stress corrosion cracking (SCC) were examined by varying phosphorus segregation and chromium depletion through controlled thermal treatments. Grain boundary enrichment of phosphorus was found to promote IG corrosion, but not SCC, of 316 SS in low-temperature, sulfuric acid solutions at transpassive potentials. Results from slow-strain-rate, straining-electrode tests at various anodic (active to transpassive) potentials show no evidence that grain boundary phosphorus enrichment (without chromium depletion) promotes IGSCC. Phosphorus segregation did promote IG hydrogen cracking at cathodic potentials. The fracture mode changed from trans-granular (TG) to IG as the phosphorus at the boundary reached about 8% of a monolayer. This fracture mode transition corresponds to a drop in ductility from approx-imately 70% strain-to-failure (<5% of a monolayer phosphorus) to 15% strain-to-failure (>8% of a monolayer phosphorus).

Chromium depletion is shown to promote IG attack at active/passive potentials in a low-temperature sulfuric acid solution and IGSCC in high-temperature water. The minimum chromium concentration at the grain boundary controlled both corrosion and cracking susceptibility for 304 SS. Grain boundary chromium minimums below about 13 wt% induced

IG attack during electrochemical potentiokinetic reactivation (EPR) experiments, while minimums up to 14 wt% prompted IGSCC in slow-strain-rate tests in 300 C oxygenated water. The transition from TG to IG fracture was mapped as a function of minimum chromium level on specimens where the depletion width was constant (~50 nm). Ductility was found to drop consistently with the decrease in chromium minimum and the increase in IG fracture. The implications of these results on current understanding of irradiation-assisted SCC is discussed.

Introduction

Irradiation-assisted stress corrosion cracking (IASCC) continues to be a problem of engineering concern for light-water reactor core components. Material microstructures and microchemistries are changed along with water chemistries due to irradiation exposure in the core. (1-5) However, very little is known about specific mechanisms that control cracking susceptibility. Preparation and testing of neutron-irradiated materials is difficult and costly. As a result, experimental evidence identifying irradiation-induced microcharacteristics and their influence on IASCC is extremely limited.

Radiation-induced segregation (RIS) to grain boundaries in stainless steel (SS) and nickel-base alloys has been implicated in IASCC. While a few measurements of RIS in neutron-irradiated SSs have been reported (3, 6-9), much of the present understanding of RIS phenomena has resulted from ion-irradiation experiments. Ions have many advantages over neutrons. The most important advantage is the difference in time and expense required to produce comparable damage. The ability to conduct detailed parametric studies and evaluate mechanistic aspects of irradiation effects are often possible with ions and not with neutrons. Ion irradiation is not without its limitations, particularly when investigating problems such as RIS to grain boundaries and IASCC. One important limitation is the shallow damage depth (microns) typically produced by ion irradiation. As a result, surface segregation measurements have been used to evaluate RIS and indicate potential grain boundary microchemistries. (10)

Phosphorus, silicon and nickel have been observed to enrich, and chromium and molybdenum to deplete, SS interfaces due to RIS. Of these elements, phosphorus, silicon and chromium are believed to have the largest effect on intergranular (IG) corrosion and IGSCC. Direct correlations between thermally-induced interfacial chemistries and SCC have been demonstrated for simple iron- and nickel-base alloys (11-14), but few comparisons have been made for SSs. Bruemmer (15,16) demonstrated that the extent of grain boundary chromium depletion controls the SCC susceptibility of 304 SS in high-temperature water. Cracking occurred as the minimum chromium content dropped below about 14 wt%. Phosphorus segregation has been shown to promote IG corrosion in highly oxidizing solutions (17,18), but had little (19) or no (20) influence on IGSCC in high-temperature water. Little is known about the influence of silicon grain boundary enrichment since it does not thermally segregate a significant amount in typical SSs.

The present work investigates RIS of chromium, silicon and phosphorus to grain boundaries and interfacial chemistry effects on IG corrosion and SCC in 304 and 316 SS. Irradiation effects on grain boundary chemistry are examined using analytical transmission electron microscopy (ATEM) of heavy-ion bombarded, fine-grained SS. Corrosion and SCC resistance are evaluated using potentiostatic tests as a function of thermally-induced interfacial chemistries.

Experimental Procedure

Materials

Four laboratory SS heats doped with phosphorus and/or silicon were cast as 34 kg ingots. These heats are designated 316-1,2,3 and 304-1 in Table 1. Material for corrosion and SCC tests was forged and rolled to plate, then solution annealed at 1100 C for 1 h and water quenched. This resulted in a grain size of about 120 μm for these heats. Specimens were subsequently heat treated at lower temperatures to establish specific microchemistries for corrosion and SCC tests. The 304-2 heat was purchased commercially as plate and heat treated as indicated above.

Solution-annealed specimens of heats 316-1 and -2 were aged for various times at 750 C to produce a series of grain boundary phosphorus compositions with (heat 2) and without (heat 1) carbide precipitation and chromium depletion. Specimens were also step cooled (800C/5h + 750C/25h + 700C/100h + 650C/150h + 600C/150h) which resulted in maximum phosphorus coverage at grain boundaries.

Sputter Deposition

Fine-grained materials for RIS studies were produced by sputter deposition techniques. Deposits of Ni-rich 316 SS were made using heats 2 and 3 as target material and of 304 SS using heat 1 as target material. Nickel plugs were inserted into the SS targets to increase the nickel concentration of the deposit to about 21 wt% and ensure that the sputtered material would be austenitic. Except for the increased nickel concentration, bulk composition of the sputter-deposited SSs were nearly identical to those listed in Table 1.

Deposition was accomplished using a triode sputtering method (21) within a metal vacuum chamber containing a tungsten filament cathode, water-cooled anode and water-cooled target. The anode substrate was polished copper, and foils of both heats 2 and 3 were made to a thickness of approximately 0.13 mm. Krypton was used as the sputter gas for initial deposits (heat 316-2), while xenon was used for the heat 316-3 and 304-1 deposits to reduce the amount of trapped gas. The copper substrate was chemically removed in dilute nitric acid. X-ray diffraction revealed the as-sputtered deposits to be predominately austenitic with trace amounts of ferrite that disappeared after heat treatment.

Grain sizes of the SS foils were extremely fine, on the order of 20 nm. Strips taken from the center of the deposit were heat treated at 750 C for 1 h to remove the as-sputtered micro-structure and establish a final grain size of about 0.3 μm. This grain size was selected so that several grain diameters would be irradiated during ion bombardment and "bulk" irradiation effects could be approximated as illustrated by the schematic in Figure 1.

Ion Irradiations

Three mm diameter discs punched from the heat treated SSs were lightly abraded and given an electrochemical polish prior to ion bombardment. Specimens were mounted in a vacuum chamber (22) and exposed to 5 MeV Ni^{++} at sufficient current to give irradiation damage from 1 to 10 displacements per atom (dpa). Damage was calculated using the computer code EDEP-1 (23) for an ion fluence of 1.8×10^{16} ions/cm^2. The total damage depth was 1.2 μm and the target depth for microstructural and microchemical analysis was between 0.4 and 0.6 μm.

Specimens were irradiated under vacuum (< 5 X 10^{-6} Pa) at a temperature of 500 C. Thermal control specimens were heated in the irradiation chamber for times equal to a 10 dpa irradiation. Dose rates for specimens were either at 0.003 or 0.005 dpa/s.

Microstructural and Microchemical Measurements

Examination of the thin damage layer required a special electrochemical thinning technique (24) to obtain electron transparent regions for analysis at the optimum depth (~0.5 μm) from the irradiated surface. Electrochemical jetting and polishing of the SS specimens were done using a 5 vol% perchloric acid-methanol solution cooled to -40 C. The depth examined from the ion-bombarded surface was measured using a stylus profilometer. Average analysis depth was 0.5 μm, but varied by about 0.1 μm across the 3 mm disc.

Elemental compositions at, and compositional profiles across, grain boundaries were measured by ATEM using a Philips EM400T TEM/STEM and an energy dispersive X-ray spectrometer (EDS). Interfacial compositions were documented in the heat-treated and irradiated conditions for the sputter-deposited SSs. STEM-EDS was also used to measure chromium depletion profiles and Auger electron spectroscopy (AES) to determine phosphorus segregation in thermally treated specimens. AES measurements were made on sample fracture surfaces using a high-resolution, PHI Model 660 Scanning Auger Multiprobe.

Methods for STEM-EDS analysis of grain boundary chemistry have been described elsewhere (25, 26) along with quantification of the X-ray spectra and estimation of error. Generally, EDS analysis in the Philips instrument was obtained in the scanning mode using a 10 nm incident electron probe. Foil thicknesses in analysis regions were from 50 to 100 nm so that through-thickness resolution was less than 20 nm. Concentration profiles were typically taken in 10 to 25 nm steps across boundaries.

Corrosion and SCC Tests

Controlled potentiostatic corrosion and slow-strain-rate SCC tests were conducted on thermally treated specimens (heats 316-1 and -2) in 1N H_2SO_4 solutions. Corrosion tests were performed for times up to 16 h at anodic potentials. A straining electrode test apparatus (11) was used for SCC tests at a constant strain rate of 1 X 10^{-6} s^{-1}. Tests were performed at anodic (passive and transpassive) and selected cathodic potentials. Corrosion potential for the SS specimens was approximately -0.3 V relative to a saturated calomel electrode (SCE). Selected electrochemical potentiokinetic reactivation (EPR) tests were also conducted to examine chromium depletion effects on IG attack. The majority of these test results have been reported previously. (27) Stress corrosion susceptibility has been evaluated by slow-strain-rate (1 X 10^{-6} s^{-1}) tests in 300 C aerated (~8 ppm O_2) water. As for the EPR results, current high-temperature water SCC work only adds several data points to results published earlier. (15)

Results and Discussion

Irradiation-Induced Grain Boundary Chemistry

Grain boundary chromium depletion as well as silicon and nickel enrichment was identified in the fine-grained SS heats after ion irradiation, while thermal-control specimens showed no

differences between interfacial and matrix compositions. The most consistently observed microchemistry change in the 316 and 304 heats was chromium depletion. After irradiation to damage levels of 5 dpa or more, nearly all boundaries showed significant depletion as compared to matrix chromium levels. A summary of data for 316 specimens irradiated to 5 or 10 dpa is presented in Figure 2 comparing measured grain boundary and matrix chromium concentrations. Measured boundary concentrations by STEM-EDS ranged from about 10.5 to 14.5 wt% versus 14 to 15.5 wt% measured in the matrix.

Chromium depletion profiles were extremely narrow at boundaries as indicated in Figure 3. The measured depletion width was less than 40 nm, but is significantly less that this due to spatial resolution restrictions. Since the through-thickness STEM-EDS resolution was on the order of 20 nm, accurate chromium minimums could not be directly determined. A better estimate of the true chromium minimum concentration and depletion width was interpolated following the approach of Was and Kruger. (28) These interpolated profiles are shown by the dashed curve in Figure 3. Chromium minimums are therefore typically several percent below analyzed values with depletion widths less than 20 nm.

Silicon was found to be enriched at many grain boundaries in both 316 and 304 heats. The most consistent results have been generated for the silicon-doped, 316-3 heat. An example of this enrichment is documented in Figure 4. STEM-EDS measurements revealed interfacial compositions up to 3.2 wt% with matrix compositions typically 1.6 wt% after ion irradiation to damage levels of 5 or 10 dpa. Lower silicon concentrations in the matrix (as compared to bulk levels) reflect the presence of large Mo- and Cr-rich silicides dispersed in the microstructure. Dilution effects again limit the ability to accurately assess boundary composition and profile width. Interpolated data shows that grain boundary silicon levels exceed 4 wt% on certain boundaries in the high-silicon 316 heat and 1.5 wt% in the 304-1 heat. Boundary-to-boundary variations in silicon enrichment were documented similar to that noted for chromium depletion (Figure 2). While some of this variability is inherent in the STEM-EDS measurement technique, the large compositional differences observed suggest that RIS depends on individual grain boundary characteristics. Equilibrium segregation and precipitation processes have been shown to directly depend on the structure and energy of grain boundaries, but such a dependence has not been documented for non-equilibrium segregation.

Preliminary results show that RIS increases with increasing ion irradiation dose up to 10 dpa. Enrichment ratios (grain boundary concentration/matrix concentration) for chromium, silicon and nickel are plotted as a function of dose in Figure 5. Chromium ratios decrease and silicon ratios increase as damage level changes from 1 to 5 to 10 dpa. A small enrichment of nickel was also seen at grain boundaries particularly in 5 and 10 dpa specimens. The behavior of these three elements is qualitatively similar to the few grain boundary chemistry measurements in neutron-irradiated SSs. Norris (3) and Jacobs, et al. (7) reported narrow chromium depletion widths and minimums definitely below bulk levels. Measured silicon enrichments ratios at boundaries are comparable to the ratio of 1.4 reported by Fukuya, et al. (6) for neutron- or electron-irradiated SS.

Phosphorus was not observed at grain boundaries in any heat even though bulk concentrations up to 0.2 wt% were present. This suggests that phosphorus enrichment is small or is highly localized at interfaces. If phosphorus is only enriched within the boundary plane (i.e. over ~ 2 atom spacings as for equilibrium segregation), then significant amounts may be present, but below STEM-EDS detectability. Phosphorus has been detected at interfaces in SSs after neutron

(3,6-9) irradiations. Enrichment ratios in 304 SS have been estimated as high as 200 from AES measurements (7), but large variations were present among IG regions analyzed. Measurements are continuing in the present work using a higher-resolution dedicated STEM, and attempts are being made to promote IG fracture in the fine-grained SS for AES determination of grain boundary chemistry.

Grain Boundary Chemistry on IG Corrosion and SCC

Many of the irradiation-induced grain boundary segregants also enrich or deplete interfaces due to thermal processes. This enables controlled interfacial chemistries to be produced in order to assess quantitatively effects on environmental degradation. Phosphorus strongly segregates to SS boundaries by an equilibrium process (16). Heat treatments in the temperature range from 500 to 700 C for 304 SS and 600 to 800 C for 316 SS can promote significant phosphorus grain boundary enrichment. Chromium depletion results from the precipitation of Cr-rich, $M_{23}C_6$ carbides and differences between chromium and carbon diffusivities. This phenomena is commonly referred to as sensitization and is prompted by heat treatments from 500 to 800 C for 304 SS and 550 to 850 C for 316 SS. The final element of interest, silicon, does not significantly segregate to SS grain boundaries and, as a result, experiments have concentrated on isolating effects of phosphorus segregation and chromium depletion on IG corrosion and SCC.

Corrosion resistance of heat-treated SSs was evaluated using two electrochemical test methods: (1) potentiokinetic reactivation by the EPR test and (2) constant potential etching in 1N H_2SO_4 solutions. Chromium depletion regions are preferentially attacked in the EPR test and the extent of depletion directly correlated with the charge transfer during the test. (27) A critical chromium concentration exists at the boundary where IG attack will occur at lower contents with no attack at higher contents. As indicated in Figure 6, this critical concentration is approximately 13 wt% for attack in the EPR test. The extent of IG attack is also a direct function of the depletion width (27), but for wide range of different widths IG attack will not occur if the minimum increases above 13 wt%. Experiments are underway to determine if a minimum chromium depletion width also exists to induce IG corrosion (and SCC) since RIS profiles are extremely narrow.

Grain boundary chromium concentration also controls IGSCC susceptibility. An example of this is presented in Figure 7 correlating fracture mode and ductility to the measured interfacial chromium content. (15) As chromium is depleted at the boundary, the fracture mode changes from TG microvoid coalesence to IG and the ductility (as indicated by the reduction in area) is significantly reduced. A critical chromium concentration of ~14 wt% can be identified as promoting IG cracking. This value is slightly greater than that determined for IG attack in the low-temperature acidic environment. Chromium minimum effects were evaluated by using specimens with comparable depletion widths (~50 nm). The depletion width may have an important effect on IGSCC susceptibility, in particular when very narrow profiles (like those for RIS) are considered. Other factors, such as solution chemistry, electrochemical potential and straining characteristics may impact this "critical" chromium concentration for IGSCC.

Grain boundary phosphorus enrichment induced IG attack at more oxidizing potentials in the H_2SO_4, constant potential exposures. IG corrosion was observed at potentials of 1.0 V (SCE) or greater, i.e. at transpassive potentials, if sufficient phosphorus was present at the boundary. Heat 316-1 specimens with low interfacial phosphorus concentrations, solution-annealed (<1% of monolayer P) and 750 C heat-treated SSs (4-8% P) revealed very little attack at 1.0

V. On the other hand, step-cooled specimens (10% P) showed definite IG penetration at this potential. The severity of attack increased with increasing transpassive potential with 750 C specimens exhibiting IG attack at 1.1 V and even the solution-annealed material showed slight grooving of boundary regions.

Step-cooled heat 316-2 specimens exhibited IG corrosion at both passive and transpassive potentials. In general, attack was more severe for these specimens since phosphorus enrichment and chromium depletion were present at boundaries. The most significant difference between heat treated 316-1 and 316-2 specimens was the observation of IG attack, even at passive potentials. This demonstrates the importance of chromium depletion at less oxidizing potentials. Phosphorus-enriched boundaries require highly oxidizing potentials to promote corrosion.

Gamma and neutron irradiation have a significant effect on the water chemistry and electrochemical conditions in the reactor core. Shifts in SS corrosion potential of +0.2 to 0.3 V have been reported. (2) Such shifts will increase the oxidizing potential of the solution, but will be less than the transpassive potentials evaluated in the H_2SO_4 corrosion tests. These present tests cannot be directly compared to high-temperature water environments; however, results do point out the increased potency of chromium depletion over phosphorus segregation in promoting IG attack.

Phosphorus-induced IG corrosion of 316 SS observed in this work is remarkably similar to that seen for phosphorus in nickel. (29) Corrosion was found at transpassive potentials when phosphorus was enriched at nickel grain boundaries. Phosphorus also prompted rapid IGSCC in nickel during slow-strain-rate straining electrode tests at transpassive and near-transpassive potentials. (13,14) However, IGSCC was not seen during comparable tests on step-cooled heat 316-1 specimens. IG corrosion and isolated IG cracks were identified during tests at 1.0, 1.1 and 1.2 V, but no significant SCC or loss in ductility was found. These results are in sharp contrast to that for nickel and probably reflect basic differences in passivation characteristics between nickel and SS.

Phosphorus segregation effects on hydrogen-induced cracking of 316 SS were quite different than observed for nickel during slow-strain-rate tests at cathodic potentials. Phosphorus segregation was found to have a small influence on HIC of nickel. (12) Tests on a step-cooled, heat 316-1 specimen at a cathodic potential of -0.6 V revealed a change in fracture mode to nearly 100% IG accompanied by a drop in the strain to failure from about 75% (at open circuit and anodic potentials) to 30%. A transition in fracture behavior from ductile TG to low-ductility IG was mapped as a function of phosphorus content at the grain boundary. This fracture mode transition and the corresponding change in ductility is shown in Figure 8. Under the conditions of this test, a critical segregation of phosphorus of about 8% of a monolayer is required to prompt IG cracking. Differences in HIC resistance may stem from differences in strength levels between low-strength pure nickel and higher-strength SSs of this study.

These results for phosphorus effects on cracking illustrate the complexity involved in environment-induced cracking processes and the need for mechanistic understanding of both material and environmental components. For tests in low-temperature H_2SO_4 solutions, phosphorus segregation is detrimental if hydrogen plays a critical role in crack growth, but does not promote IGSCC at anodic potentials where active-path dissolution might be expected. Somewhat conflicting results have been reported for phosphorus effects in high-temperature-

water SCC tests. Andresen and Briant (20) saw no detrimental effect of phosphorus grain boundary enrichment, while Jacobs (19) reported a slight tendency for IGSCC with segregated phosphorus.

Chromium depletion will have a dominant influence on IGSCC in oxidizing high-temperature water if sufficient depletion is present. Irradiation can produce nonequilibrium grain boundary chromium contents below the critical value necessary for SCC resistance. However, it is not known whether sufficient depletion occurs during neutron exposure in-core to explain the observed dose threshold for IASCC. In addition, the unique aspects of grain boundary chemistry produced by RIS, i.e., narrow chromium depletion profiles with no intergranular carbides, simultaneous enrichment of other elements such as silicon, and a sharp increase in matrix strength level, makes it difficult to assess response based on more conventional thermally induced microchemistries.

Conclusions

Irradiation-induced grain boundary chromium depletion and silicon enrichment have been observed in fine-grained, 316 and 304 heats after ion bombardment at 500 C. Measured chromium levels dropped from more than 15 wt% in the matrix to as low as 8 wt% at boundaries. Silicon increased by a factor of 3 to 4 times over the matrix. Compositional changes were localized within about 10 nm of the interface. Enrichment ratios for chromium, silicon and nickel were found to change consistently with ion irradiation dose up to 10 dpa. Phosphorus enrichment was not documented in any of the SS heats even though heats contained high concentrations in the bulk.

Direct correlations have also been made between thermally induced grain boundary chemistries and both IG corrosion and SCC. Minimum interfacial chromium concentrations were shown to control IG corrosion in a low-temperature acidic environment and IGSCC in high-temperature water. Critical chromium concentrations were identified to induce IG corrosion (~13%) and IGSCC (~14%) based on these experiments. Phosphorus segregation promoted IG attack only at transpassive potentials in sulfuric acid, while chromium depleted regions were attacked at passive and transpassive potentials. Although phosphorus promotes IG corrosion, no evidence of IGSCC was observed in slow-strain-rate, straining electrode tests at anodic potentials. Phosphorus segregation did promote hydrogen-induced cracking in tests at cathodic potentials but required a grain boundary composition of about 8% of a monolayer to initiate cracking.

Acknowledgments

The assistance of M. D. Merz and B. W. Arey is gratefully acknowledged. Constructive discussions with J. L. Nelson of the Electric Power Research Institute (EPRI) are also appreciated. This work was partially supported by EPRI and by the Office of Basic Energy Sciences, U.S. Department of Energy under Contract DE-AC06-76RLO 1830.

References

1. H. Hanninen and I. Aho-Mantilla, Proc. Third Int. Sym. on Environmental Degradation of Materials in Nuclear Power Systems - Water Reactors, Eds., G. J. Theus and J. R. Weeks, The Metallurgical Society, Warrendale, PA, 1988, p. 77.
2. P. L. Andresen and F. P. Ford, Proc. Corrosion 89, National Association of Corrosion Engineers, Paper 497, 1989.
3. D. I. R. Norris, ed. Proc. Sym. Radiation-Induced Sensitization of Stainless Steels, Berkeley Nuclear Laboratory, CEGB, INIS-GB-90, 1986.
4. F. Garzarolli, D. Alter, P. Dewes and J. L. Nelson, ibid ref 1.
5. A. J. Jacobs, G. Wozado, K. Nakata, T. Yoshida and I. Masaoka, ibid ref 1.
6. K. Fukuya, S. Nakahigashi, M. Terasawa and S. Shima, ibid ref 1.
7. A. J. Jacobs, R. E. Clausing, L. Heatherly and R. M. Kruger, 14th Annual ASTM Sym. Radiation on Materials, Andover, MA, 1988.
8. R. E. Clausing and E. E. Bloom, in Grain Boundaries in Engineering Materials, Claitors, Baton Rouge, LA, 1975, p. 491.
9. F. Farrell, N. Kishimoto, R. E. Clausing, L. Heatherly and G. L. Lehman, J. Nucl. Mat., Vols. 141-143, p. 991 (1986).
10. J. L. Brimhall, D. R. Baer and R. H. Jones, J. Nucl. Mat., Vol. 103-104, p. 1379 (1981); Vol. 117, p. 218 (1983); Vol. 122-123, p. 196 (1984).
11. R. H. Jones, S. M. Bruemmer, M. T. Thomas and D. R. Baer, Met. Trans., Vol. 12A, p. 1621 (1981).
12. S. M. Bruemmer, R. H. Jones, M. T. Thomas and D. R. Baer, Met. Trans., Vol. 17A, p. 1429 (1983).
13. S. M. Bruemmer, R. H. Jones, D. R. Baer and M. T. Thomas, Proc. Corrosion 81, National Association of Corrosion Engineers, Paper 243, 1981.
14. R. H. Jones, M. J. Danielson, S. M. Bruemmer, D. R. Baer and M. T. Thomas, Proc. Int. Sym. Embrittlement by the Localized Crack Environment, The Metallurgical Society, Warrendale, PA, 1984.
15. S. M. Bruemmer, Corrosion, Vol 44, No. 6, p. 365 (1988).
16. S. M. Bruemmer, in Grain Boundary Chemistry and Intergranular Fracture, Eds. G. S. Was and S. M. Bruemmer, Trans. Tech. Publ., Aedermannsdorf, Switzerland, in press.
17. C. L. Briant, Met. Trans., Vol. 16A, p. 2061 (1985).
18. C. L. Briant, Met. Trans., Vol. 18A, p. 691 (1987)
19. A. J. Jacobs, ibid ref 2, Paper 495.
20. P. L. Andresen and C. L. Briant, ibid ref 1, p. 371.
21. S. D. Dahlgren, Met. Trans. Vol. 1, p. 3095 (1970).
22. H. E. Kissinger, J. L. Brimhall, E. P. Simonen and L. A. Charlot, PNL-2594, Pacific Northwest Laboratory, Richland, WA, 1978.
23. I. Manning and G. P. Mueller, Comp. Physics Comm., Vol. 7, p. 85 (1974).
24. H. Brager, H. E. Kissinger and G. L. Kulcinski, Rad. Effects, Vol. 5, p. 781 (1970).
25. S. M. Bruemmer and L. A. Charlot, Scripta Met., Vol. 20, p. 1019 (1986).
26. S. M. Bruemmer, L. A. Charlot, M. T. Thomas and R. H. Jones, EPRI RD-3859, Vol. 1, Electric Power Research Institute, Palo Alto, CA, 1985.
27. S. M. Bruemmer, Corrosion, Vol. 44, No. , p. 328 (1988).
28. G. S. Was and R. M. Kruger, Acta Met., Vol. 33, No. 5, p. 841, 1985.
29. S. M. Bruemmer, R. H. Jones, M. T. Thomas and D. R. Baer, Proc. Int. Conf. Environmental Degradation of Engineering Materials, Eds. M. R. Louthan, R. P. McNitt and R. D. Sisson, Jr., Virginia Polytechnic Institute, Blacksburg, VA, p. 25, 1982.

Table 1. Compositions of SS Heats, wt%

Heat	C	P	Cr	Ni	Mo	Mn	Si	S
316-1	0.002	0.067	16.0	13.2	2.0	1.6	0.6	0.01
316-2	0.060	0.061	16.6	12.1	2.0	1.9	0.7	0.01
316-3	0.005	0.220	20.3	13.9	2.0	1.5	2.0	0.01
304-1	0.005	0.065	18.5	8.5	-	1.2	0.6	0.01
304-2	0.062	0.013	18.5	8.8	0.2	1.7	0.4	0.01

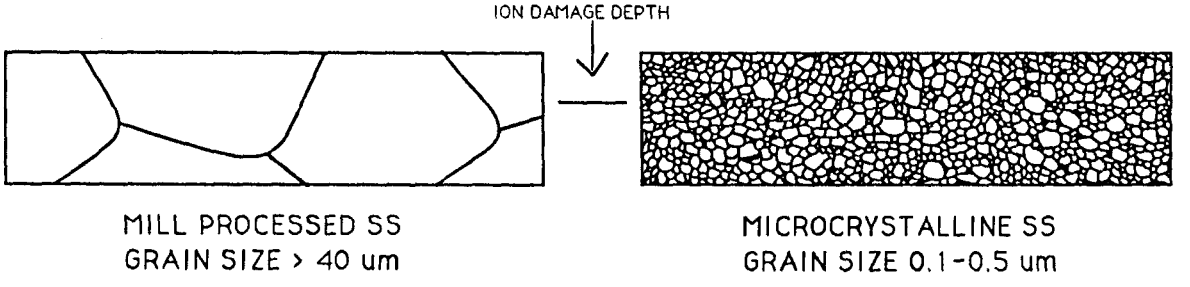

Figure 1. Schematic illustrating "bulk" damage that can be produced in fine-grained SS versus surface damage in mill-processed SS.

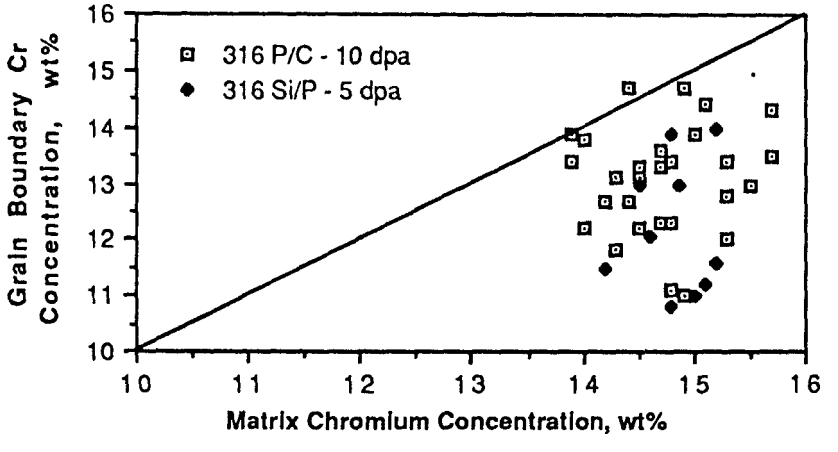

Figure 2. Grain boundary versus matrix chromium concentration measurements in ion-irradiated 316 SS specimens.

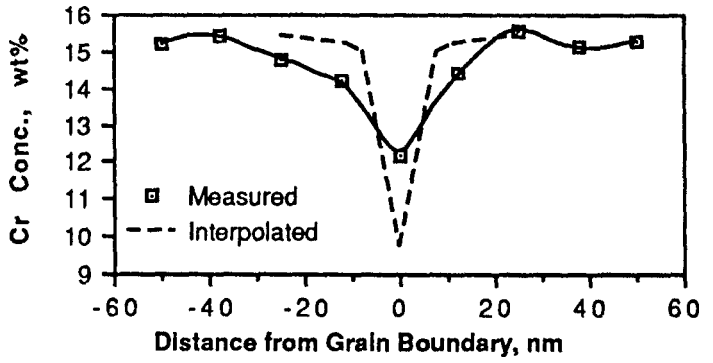

Figure 3. Measured and interpolated chromium depletion profiles in irradiated 316 SS to a damage level of 5 dpa at 500 C.

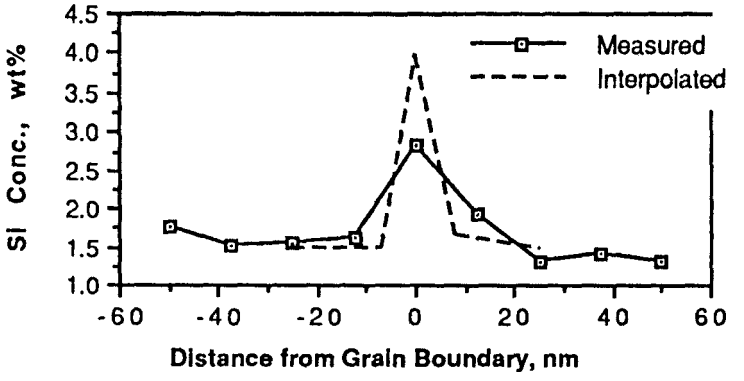

Figure 4. Measured and Interpolated silicon enrichment profiles in irradiated 316 SS to a damage level of 5 dpa at 500 C.

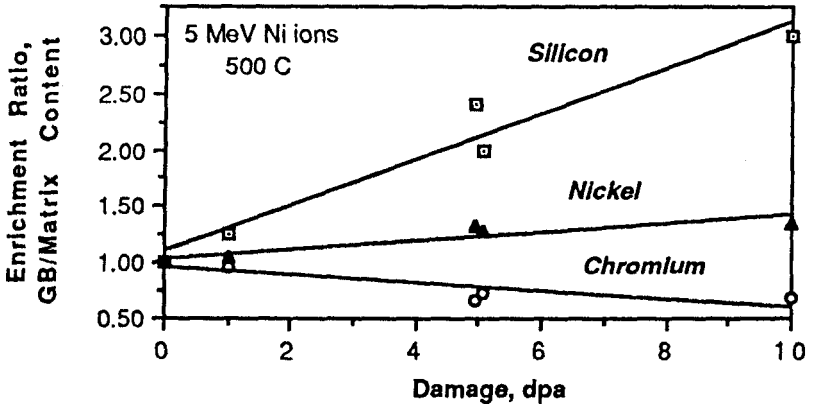

Figure 5. Measured RIS for silicon, nickel and chromium in 316 SS as a function of ion-induced damage at 500 C.

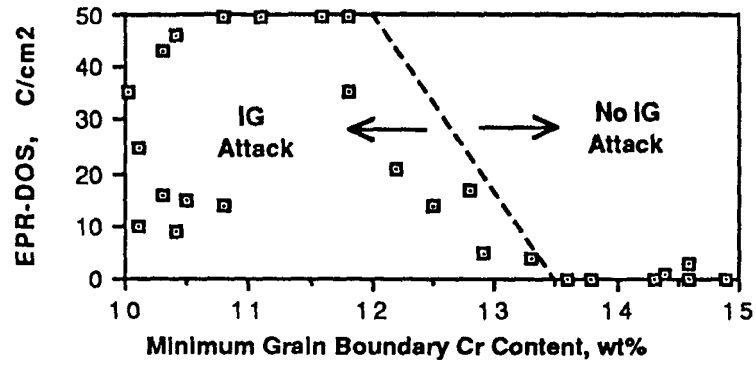

Figure 6. Comparison between grain boundary Cr depletion and extent of intergranular attack in EPR test.

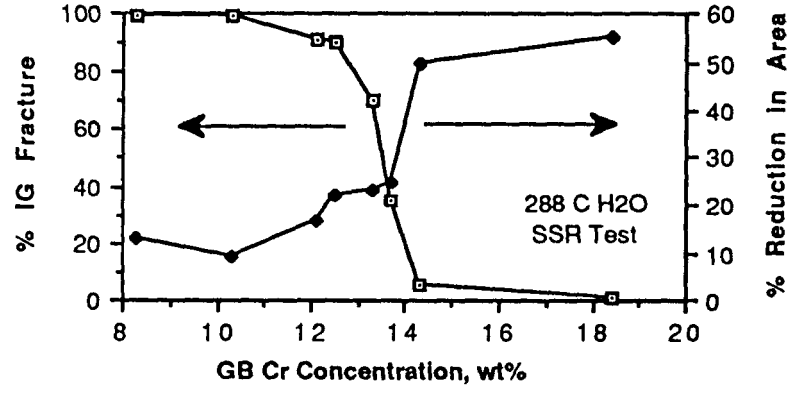

Figure 7. Grain boundary Cr concentration effects on IGSCC of 304 SS in a high-temperature water environment.

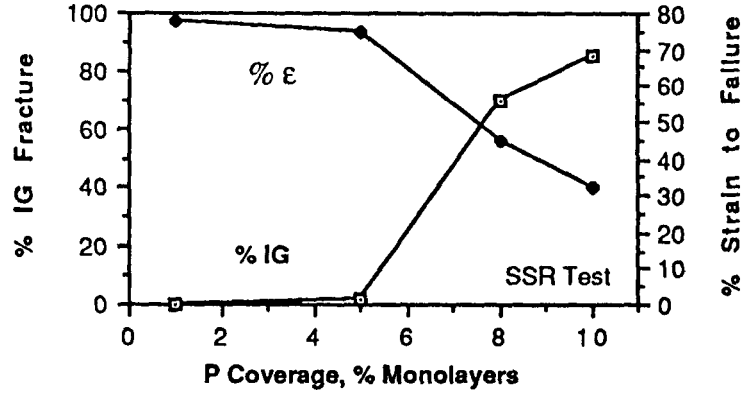

Figure 8. Phosphorus segregation effects on hydrogen-induced cracking of 316 SS.